Supplement of Geosci. Model Dev., 18, 8663–8678, 2025 https://doi.org/10.5194/gmd-18-8663-2025-supplement © Author(s) 2025. CC BY 4.0 License.





## Supplement of

# Data-driven estimation of the hydrologic response using generalized additive models

Quentin Duchemin et al.

Correspondence to: Paolo Benettin (paolo.benettin@unil.ch)

The copyright of individual parts of the supplement might differ from the article licence.

### S1 In-depth analysis for six Swiss catchments

Here we provide a detailed analysis of the six real-world catchments that were analyzed and briefly introduced in Section 2.2 of the main body of the paper.

The catchments' size, elevations and mean slope were derived from the 2-m resolution digital elevation model of Switzerland, provided by Swisstopo Swiss Federal Office of Topography.

The southern nivo-pluvial regime of Lavertezzo is characterized by two mean monthly high flows (brown curve in Figure 4b): the highest in May, driven by snow-melt (around 330 mm), and the other occurring in November, due to high precipitation (around 210 mm). Although precipitation during summer exceeds the annual average (Figure 4a), high summer evaporation rates result in generally low flows from June to October (Figure 4c). Similar behaviour occurs in the southern pluvio-nival basins, Magliaso and Chiasso (orange and purple curves respectively in Figure 4), with the highest streamflows (180 and 120 mm, respectively) arising in November due to high precipitation rather than snowmelt processes. The Euthal catchment, in the Northern Alps, is characterized by a nival transition regime with high monthly flows in May (250 mm) due to snowmelt and a secondary peak in monthly flows in August (170 mm) due to high precipitation (light blue curves in Figure 4). The Salmsach basin is typical of a pluvial regime with high mean monthly streamflows from December to June (the maximum flow occurs in December) and low flows from July to November. This is likely due to the homogeneous precipitation across the year (shown by the red curve in Figure 4a, which is the flattest with the lowest values, ranging from around 50 to 135 mm per month) but high changes in potential evapotranspiration rate due to temperature variability (as shown by the red curve in Figure 4c, with the highest values in summer of almost 120 mm per month). The streamflow in Sonceboz, with a Jura-nivopluvial regime, is driven by similar dynamics, especially by a low variance in precipitation during the year (from 85 to 155 mm per month). However, for Sonceboz the potential evapotranspiration reaches the maximum value in July with more than 100 mm per month, but it varies less than in Salmsach with the consequent effect of a higher variance in streamflow during the year and two maximum values when the potential evapotranspiration is not high (December and March, both with about 140 mm per month).

The basins exhibit considerable variation in catchment topography, as illustrated in the panels of Figure 3 and detailed in Table 1. Magliaso and Chiasso span a wide range of altitudes, from approximately 300 m a.s.l. to over 1600 m a.s.l.. In contrast, Euthal is mainly located at higher elevations, ranging from around 900 to 2200 m a.s.l., similarly to Sonceboz with portions of area between 600 and 1600 m a.s.l.. The Salmsach basin, on the other hand, features a more uniform elevation between 400 and 500 m a.s.l.. Lavertezzo displays high-relief terrain typical of alpine environments, with sections exceeding 2500 m a.s.l., while its channel bed lies primarily around 500 m a.s.l..

The topographic structure of these basins also reflects distinct differences in catchment-wide mean slope. Salmsach is relatively flat, whereas Sonceboz and Euthal have moderate slopes averaging between 15° and 20°. The southern-alpine basins, including Lavertezzo, Magliaso, and Chiasso, are distinguished by steeper slopes ranging from 28° to 38°.

#### S2 Three-compartment conceptual model

The benchmark model employed to create synthetic streamflow data is a simple three-box conceptual framework designed to simplify the hydrological dynamics of a real-world catchment (see Figure S1 for a schematic representation). This model extends the two-box approach previously employed in Kirchner (2016) and Kirchner (2019), which was primarily developed to infer catchment transit times. In contrast, the three-box model presented differs from the earlier models in three key ways: (i) it introduces a third box representing a channel, ii) its partitioning coefficients ( $\eta_{OF}$  and  $\eta_{SS}$  in Figure S1) can vary according to the storage level in the boxes, and (iii) it incorporates evapotranspiration processes.

The catchment in this model is represented by three compartments: the upper box, which represents soil water storage; the lower box, which represents the groundwater compartment; and a channel, which collects overland flow, subsurface flow, and groundwater discharge and converts the total contribution into stream discharge. Each box (upper, lower and channel box) is assumed to be well-mixed, meaning that the age distribution of the water in the box is equal to the one of the water that leaves the box.

In this framework, precipitation is split with a partition coefficient  $(\eta_{OF})$  into the fraction directed to the upper box  $(p(1 - \eta_{OF}))$  and the remaining portion  $((p\eta_{OF}))$  infiltrates onto the channel box. The upper box drains into the channel box with

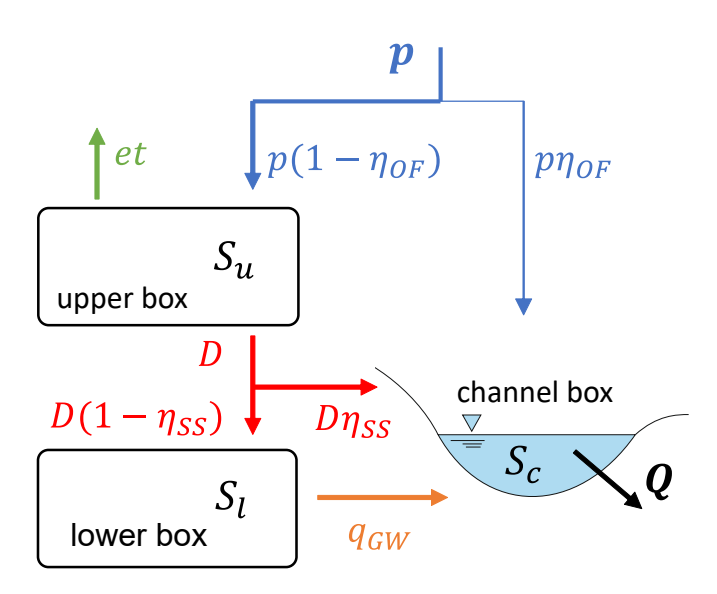


Figure S1. Schematic diagram of the three-box benchmark model. Drainage from the upper and lower boxes, along with the drainage from the channel box (converted in stream discharge) are determined by power functions depending on the storage volumes and the reference state conditions. The partition coefficients ( $\eta_{OF}$  and  $\eta_{SS}$ ) split the precipitation or the upper box drainage into contributions directed to the various boxes.

a drainage rate  $D\eta_{SS}$ , according to a power function based on its storage. The remaining portion of water leakage from the upper box  $(D(1-\eta_{SS}))$  recharges the lower box. Thus, the evolution of storage  $s_u$  in the upper box is defined as follows:

$$\frac{ds_u}{dt} = p(1 - \eta_{OF}) - et - D \tag{S1}$$

where the evapotranspiration rate is computed through the potential evapotranspiration time series and defined as  $et = Pet \times clip \left[\frac{s_u - s_{wp}}{s_o - s_{wp}}\right]_0^1$  where  $s_o$  represents the storage at which evapotranspiration is independent of storage, and  $s_{wp}$  indicates the storage under which there is no evapotranspiration. The leakage rate from the upper box is defined as  $D = D^{ref} \times \left(\frac{s_u}{s_u^{ref}}\right)^{b_u}$  (see below for the definition of the reference state denoted by ref).

The lower box is ruled by the same concept, collecting the leakage from the upper box and recharging the channel with the groundwater flow, as follows:

$$\frac{ds_l}{dt} = D(1 - \eta_{SS}) - q_{GW} \tag{S2}$$

where the groundwater flow itself is defined as  $q_{GW} = q_{GW}^{ref} \times \left(\frac{s_l}{s_l^{ref}}\right)^{b_l}$ . In the end, the channel box stores water from the various sources and the drainage from this box becomes stream discharge  $(Q = Q^{ref} \left(\frac{s_c}{s_c^{ref}}\right)^{b_c})$ , with the following rule:

$$\frac{ds_c}{dt} = p\eta_{OF} + D\eta_{SS} + q_{GW} - Q \tag{S3}$$

The partitioning coefficients for the overland flow and the shallow subsurface flow are defined with power functions of the storage of the boxes:  $\eta_{OF} = \left(\frac{s_u}{s_u + s_v^{ref}}\right)^{a_{OF}}$  and  $\eta_{SS} = \left(\frac{s_l}{s_l + s_v^{ref}}\right)^{a_{SS}}$ .

The model requires nine parameters to be fixed: the equilibrium storage levels of the upper, lower, and channel boxes  $(s_{u,ref},s_{l,ref},s_{c,ref})$ ; their respective drainage exponents  $(b_u,b_l,b_c)$ ; two partitioning coefficients, which define the fractions of discharge in the reference state from overland flow  $(f_{OF})$  and shallow subsurface flow  $(f_{SS})$ ; and the fraction of the upper box storage over which evapotranspiration is sensitive to storage level  $(f_W)$ . The "reference" state of the model represents the case where the storage levels at which the drainage rates of each box will equal their long-term average input rates. The same approach was adopted also in the applications of the two-box model and more details about the reference state can be found in Section 2.2 in Kirchner (2016). The fraction coefficients at the reference state are then defined as  $f_{OF} = \frac{q_{OF}}{q}$ ,  $f_{SS} = \frac{q_{SS}}{q}$ , and

$$1 - (f_{OF} + f_{SS}) = \frac{q_{GW}}{q}). \text{ Where } q = (1 - f_{ET})\overline{p}; f_{ET} := \left(\left(\frac{\overline{p}}{Pet}\right)^2 + 1\right)^{-1/2} \text{ and } D^{ref} = (1 - f_{ET})(1 - f_{OF})\overline{p}.$$

This conceptual model was therefore employed to create synthetic streamflow data from input precipitation and potential evapotranspiration time series. Precipitation data were available for Lugano at hourly resolution for 40 years, starting from 1980, while daily potential evapotranspiration was computed from daily air temperature (mean, minimum and maximum) using the Hargreaves method from Hargreaves and Samani (1985) (implemented through the Python Pyeto package https://github.com/woodcrafty/PyETo) and then uniformly distributed across each day at hourly intervals. The baseline synthetic dataset was generated by fine-tuning the model parameters to approximate the streamflow conditions observed at the Chiasso (Ponte di Polenta) gauging station, yielding a time series with an RMSE of 0.20 mm h <sup>-1</sup>. These parameters were further adjusted to simulate more damped and flashy hydrological responses, as outlined in Table S1. The streamflow time series generated for all three scenarios are displayed for one example year (2010) in Figure 2.

Table S1. Main parameters for the three-compartment conceptual model to simulate the different synthetic time series

Parameters	Synthetic case A (base)	Synthetic case B (damped)	Synthetic case C (flashy)
$b_u$	40	20	50
$b_l$	6	6	2.24
$b_c$	1.5	1.5	1.5
$s_{u,ref}$	100	100	294.83
$s_{l,ref}$	1000	1000	24
$egin{aligned} b_c \ s_{u,ref} \ s_{l,ref} \ s_{c,ref} \end{aligned}$	5	20	1.74
$f_W$	1.30	1.10	1.06
$f_{OF}$	0.10	0.50	0.13
$f_{SS}$	0.60	0.30	0.55

#### S3 Additional figures

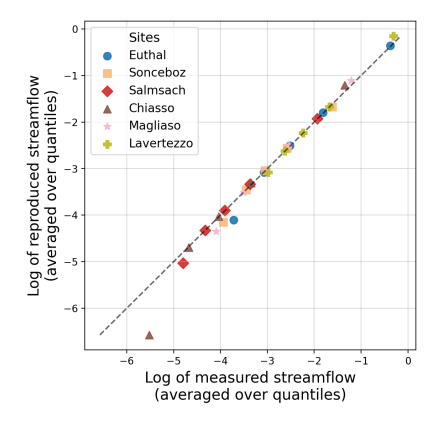


**Figure S2.** Log reproduced streamflow estimated through GAMCR for the six investigated sites as function of the log measured streamflow. The values are represented averaged over the quantiles of the entire time series.

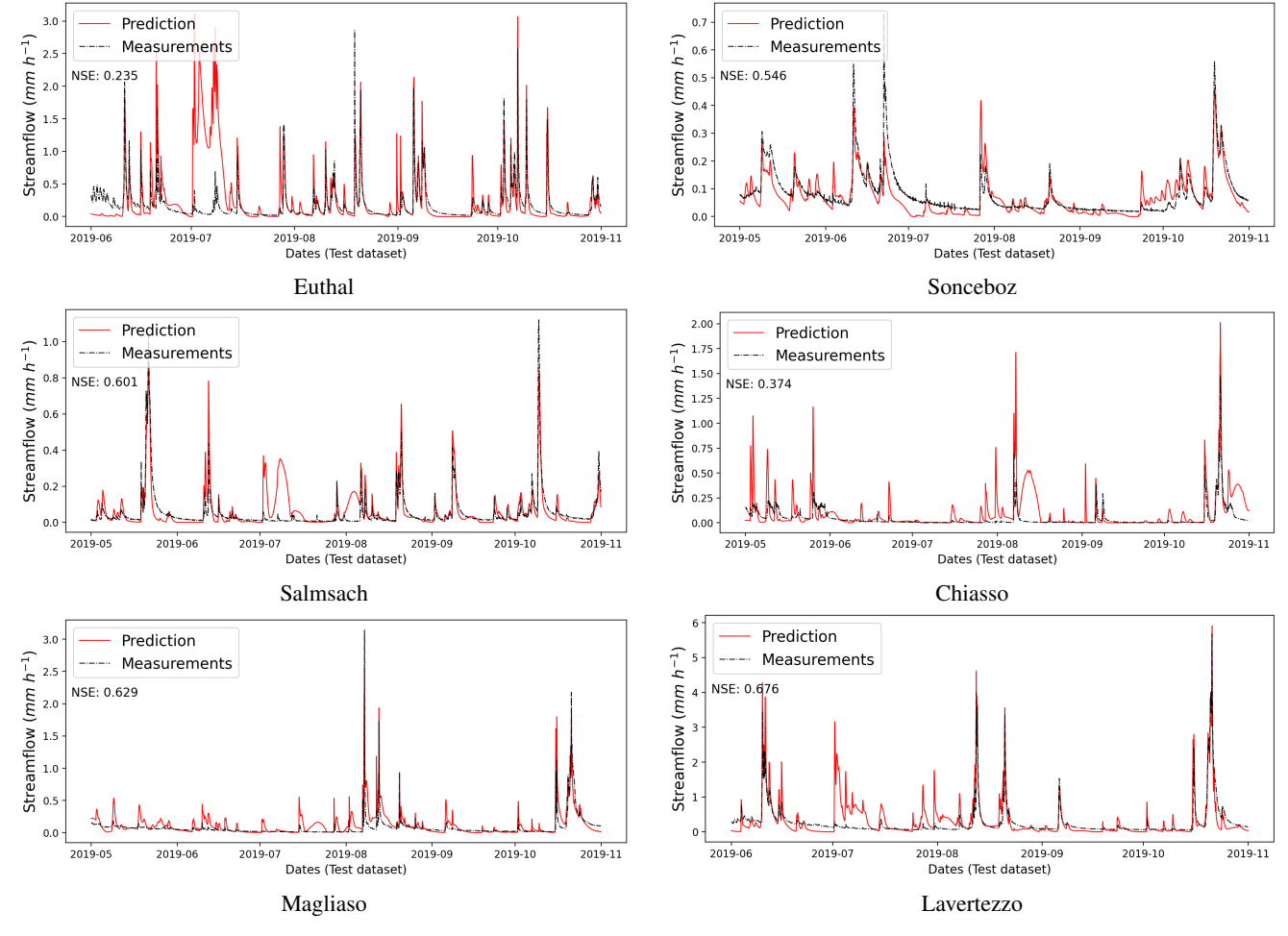


Figure S3. Reproduced hydrographs using GAMCR and streamflow measurements over the test set for the six different sites.

#### References

- Hargreaves, G. H. and Samani, Z. A.: Reference crop evapotranspiration from temperature, Applied engineering in agriculture, 1, 96–99, 1985.
  - Kirchner, J. W.: Aggregation in environmental systems Part 2: Catchment mean transit times and young water fractions under hydrologic nonstationarity, Hydrology and Earth System Sciences, 20, 299–328, https://doi.org/10.5194/hess-20-299-2016, 2016.
  - Kirchner, J. W.: Quantifying new water fractions and transit time distributions using ensemble hydrograph separation: theory and benchmark tests, Hydrology and Earth System Sciences, 23, 303–349, https://doi.org/10.5194/hess-23-303-2019, 2019.
  - Swiss Federal Office of Topography: swissALTI3D, https://www.swisstopo.admin.ch/en/height-model-swissalti3d.